Multi-Physical Design of a Wave Spring Connector for a Highly-Reliable GaN Power Module

Lei Wang
University of Twente
Enschede, The Netherlands
l.wang-10@utwente.nl

Wenbo Wang
Yongjiang Laboratory
Ningbo, China
wenbo-wang@ylab.ac.cn

Raymond J.E. Hueting
University of Twente
Enschede, The Netherlands
r.j.e.hueting@utwente.nl

Gert. Rietveld
University of Twente &
Van Swinden Laboratorium (VSL)
Enschede, The Netherlands
g.rietveld@utwente.nl

2022 IEEE International Power Electronics and Application Conference and Exposition (PEAC) | 978-1-6654-9141-9/22/$31.00 ©2022 IEEE | DOI: 10.1109/PEAC56338.2022.9959435

***Abstract*—Conventional wire bonding in emerging wide bandgap (WBG) semiconductor devices employed in power modules is subjected to failure due to thermo-mechanical stress occurring at the joints. Pressure contact technology improves the reliability of such power modules, eliminating wire bonds between the substrate and components. This paper presents the characteristics and design process of a new type of spring connector in a gallium-nitride (GaN) DC-DC converter for reducing parasitics as well as improving heat dissipation and mechanical stability. Using analytical models and multi-physics finite element method (FEM) simulations, the geometrical design of the spring has been optimized to achieve low parasitics and satisfactory cooling ability, combined with a safe maximum stress. FEM simulations and initial measurement of the optimized spring connector indicate a low inductance (~3 nH) and a low resistance (~5 mΩ).**

Keywords—connector, pressure contact, power module, reliability, WBG, multi-physical field simulation

I. INTRODUCTION

The emerging demand of green energy has dramatically driven the application of power modules in electrical vehicles, aerospace, and solar/wind power plants under extremely harsh operating environments. Highly-reliable power modules are therefore desired by the industry. The reliability of power modules depends on various factors, such as packaging approaches, the used materials and match of the thermal expansion coefficient (CTE) between those materials [1]. The physical connections between components are the most susceptible parts that should be taken into consideration [2].

Conventional wire bonds are widely applied in commercial power modules as interconnections. However, fatigue of wire bonds is the root cause of the failure in power modules, due to the fact that thermo-mechanical stress is generated at the welding points between the bond pads and wires during power and thermal cycling [2]. Bond wire heel crack and lift-off can occur since the metal (gold, aluminum, copper) wires are not able to handle large temperature swings. Moreover, with the continuous increasing power level and switching frequency of WBG devices, the reduction of parasitics has become a significant challenge in existing packaging technologies [3]. Wire bonds bring additional parasitic inductances of higher than 10 nH, which are not compatible with the high switching frequencies of WBG chips.

Pressure contact packaging is an appropriate approach that replaces wire bonds and soldering by elastomeric elements to improve the reliability of power modules. This approach provides advantages in: (1) reduced parasitic inductance due to absence of wire bonds, (2) improved reliability as prevention of failure of lift-off and heel crack at soldering layers in wire bonds, and (3) double-sided cooling since connectors also transfer heat on the top side of chips.

There have been several reports in which the full advantages of pressure contact technology in WBG devices have been utilized. For example, J. Gonzalez *et al*. explored the feasibility of pressure contact on SiC chips and developed a 200 A SiC Schottky diode power module to study the influence of pressure on the current distribution and forward voltage [4]. N. Zhu *et al*. used flexible press pins called "fuzz button" in a low-profile interposer to apply pressure contacts on the top side of SiC MOSFETs [5]. Their experiment shows that the internal stray inductance of their half-bridge power module is less than 4.3 nH at a frequency of 100 kHz. In [6], springs were used as terminals in a wire-bond-less 10 kV SiC MOSFET power module to conduct current between the direct bond copper (DBC) and bus bar. High-speed switching of 250 V/ns was achieved with negligible ringing and voltage overshoot.

Application of pressure contact packaging in commercial silicon (Si) insulated-gate bipolar transistor (IGBT) power modules can be divided into two types: Press pack and Stakpak. The former is a direct rigid contact method, where molybdenum (Mo) plates pressed by an external clamping force are placed between an electrode and chips. Companies like Westcode and Semikron widely utilize press pack IGBT modules in high voltage (HV) direct current (DC) transmission and alternating current (AC) transmission

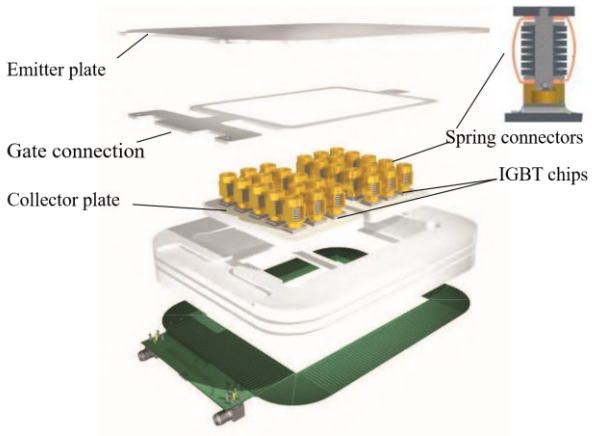

Figure 1: Spring connectors in a Stakpak module with Si IGBTs.

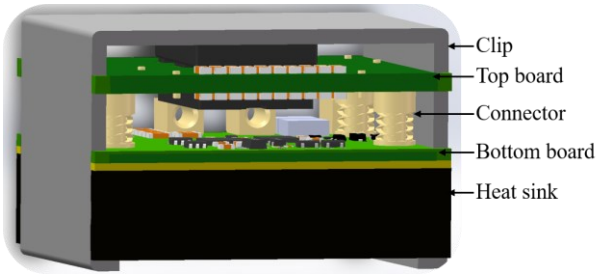

Figure 2: Proposed application of the proposed wave spring connectors in a GaN DC-DC converter.

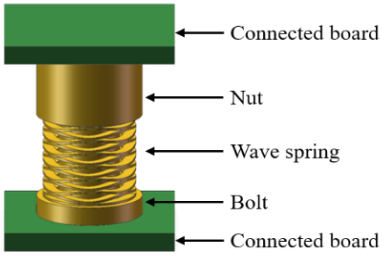

Figure 3: Structure of the proposed wave spring connector.

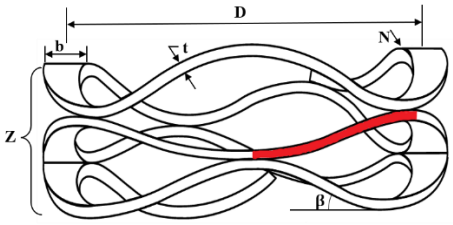

D: Mean diameter

Z: Number of turns

N: Number of waves per turn

b: Radial width of cross section

t: Thickness of cross section

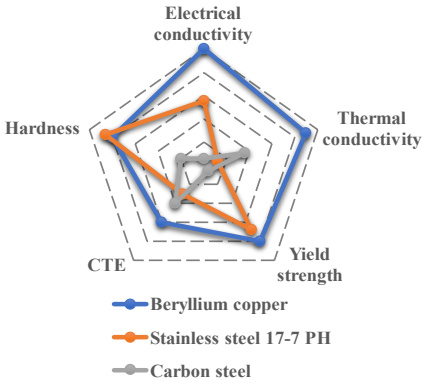

Figure 5: Qualitative comparison of physical properties of commonly-used spring materials.

systems [7]. However, the direct rigid contact requires strong control over surface roughness, structure deformation, and manufacturing tolerance, since the pressure affects the electrical and thermal contact resistance [8]. Hitachi Energy uses spring connectors as a soft contact packaging technology in discrete IGBT products, named Stakpak [9]. In a Stakpak module, the electric pole board provides an external force to press dies through a series of uniformly arranged hard springs and the current can flow through a bypass from dies to the board. Fig. 1 illustrates the spring system between the IGBT chips and emitter plate in such a Stakpak module. Compared with a press pack module, the pressure of individual chips in a Stakpak module can be adjusted by the spring constant f to compensate the inhomogeneity of the clamping force for a balanced distribution. This approach offers improved reliability during thermal cycling compared to wire bonding and soldering, because the soft springs absorb the additional stress energy when components made from different materials deform.

Although spring connections have been incorporated in IGBT modules for many years, they have not yet been used in GaN power modules. The relatively small size and homogeneous horizontal structure of GaN chips add complexity in the realization of pressure contacts in GaN power modules [4]. The requirement of low parasitics and thermal conductance also limits the usage of conventional mechanical clips and springs. Conventional coil springs induce a too high inductance and resistance. With the increasing power level and switching frequency of WBG semiconductor devices, the reduction of parasitics has become a serious challenge in existing packaging approaches. Researchers have investigated other approaches to connect chips with board pads, *e.g.*, fuzz button, post, and metal foam [5, 10, 11]. However, so far such designs have only been used in SiC modules, where the working frequency is one order of magnitude lower than that in GaN modules. It is therefore important to design reliable functional connectors that are suited for the higher switching frequencies in GaN modules.

This paper presents a design and optimization guideline for the important parameters of a new wave spring connector for applications in GaN power module, taking into account the performance in electrical, thermal, and mechanical aspects. Fig. 2 presents its envisaged application in a 500 W 1 MHz GaN DC-DC converter, integrated in a 3D package. The connectors not only conduct current between substrates, but also spread heat from the bottom board, where GaN dies are attached to, to the top board and balance mechanical stresses. The paper is organized as follows. First, the proposed connector design is introduced. The second part investigates the impact of the material properties and geometrical parameters of the wave spring on the electrical resistance via analytical expressions. Then, multi-physics FEM simulations are discussed to study the electrical resistance, inductance and thermal properties, as well as the mechanical stress. Finally, some experiments are discussed to validate the analytical and simulation results.

II. STRUCTURE AND MATERIAL DESIGN OF THE SPRING CONNECTOR

The designed connector consists of three parts: a fixed bolt, a fluctuating spring and a moving nut (Fig. 3). The wave spring is a flexible element with a number of peaks and valleys formed by a coiled flat wire. It is used as elastic supports in pumps and linear actuators in robotic arms, but is re-designed as a connector in GaN power modules [12]. Compared with a conventional coil spring, the wave spring has several advantages:

1) The axial space can be reduced by up to 50%.
2) The mechanical load is 100% transferable in the axial direction.

TABLE I: MATERIAL PROPERTIES OF BERYLLIUM COPPER

Electrical conductivity (S/m)	Thermal conductivity (W/mK)	Yield Strength (MPa)	CTE (ppm/℃)	Hardness (HRC)	Young's Modulus (GPa)	Mass Density (g/cm^3)
1.67×10^7	120	1140	16.7	40	125	8.25

TABLE II: PARAMETERS OF THE OPTIMIZED WAVE SPRING

Diameter D (mm)	Thickness t (mm)	Width b (mm)	Turns Z	Number of waves N	Load P (N)	Free Height (mm)	Working Height (mm)	Spring Constant k (N/mm)
4.37	0.13	0.55	14	3.5	5 - 10	4.58	3.3	3.9 - 7.8

3) The current can flow from crest to crest in vertical direction. Therefore, the inductance and resistance of the wave spring are smaller than that of a coil spring.
4) It can accommodate a higher thrust load as only the wire size, number of waves/turns, and wave height need to be adjusted.

The spring is placed around the bolt, with the bolt fitting in the circular shaped hole of the nut, so that movements in horizontal direction are confined. When an external load is applied, the upper board moves downwards to force the spring in contraction as the bolt is tightly attached to a rigid bottom board. The geometrical shape of the wave spring is defined by five parameters, as shown in Fig. 4, with D the mean diameter, Z the number of turns, N the number of waves per turn, b the radial width of the metal strip, and t its thickness. β represents the angle between the spring wire and plane normal to the spring axis. Since manufacturers use a relatively small value for angle β (normally 12 degrees), the effective length l of the spring per turn can be expressed as $l \approx \pi D$. The sectional area A of the spring wire is written as $A = bt$.

Fig. 5 compares the physical properties of traditional materials used for wave springs as supplied by the spring manufacturer Smalley [12]. Apart from having a slightly higher CTE than stainless steel and carbon steel, beryllium copper ($BeCu_2$) performs excellently from a view point of both electrical and thermal conductivity (Table I). Therefore, $BeCu_2$ has been selected as the material of the connector. To reduce corrosion effects and prevent oxidation, a gold layer is electroplated on the surface of the connector. Moreover, the electroplated layer makes the surface of the machined connectors smoother, thereby reducing contact resistances between the connectors and boards.

III. PARAMETER OPTIMIZATION

The design of the wave spring requires a multi-physical approach to simultaneously optimize the electrical, thermal and mechanical properties. The contact points at the crests of the waves influence both the electrical and thermal resistance. Since the spring is compressed during operation, ideal contacts at the crests are assumed so that the wave spring can be split into elements of length $l = \pi D/2N$. The red area in Fig. 3 highlights such an element. A number of $2N$ elements connected in parallel form a complete single turn, and a number of Z turns connected in series form the whole spring. The deformation factor C is defined by the ratio of deformed height to the free height, *i.e.*, C equals to 1 when the wave spring is free. C also contributes to the resistance since larger contraction enlarges the effective connection areas at the crests, resulting in a shorter current flow path. To simplify the calculation, C is assumed to be equal to the ratio of working height and free height. There is a negligible mutual inductance in the proposed spring as each turn is divided into several arcs,

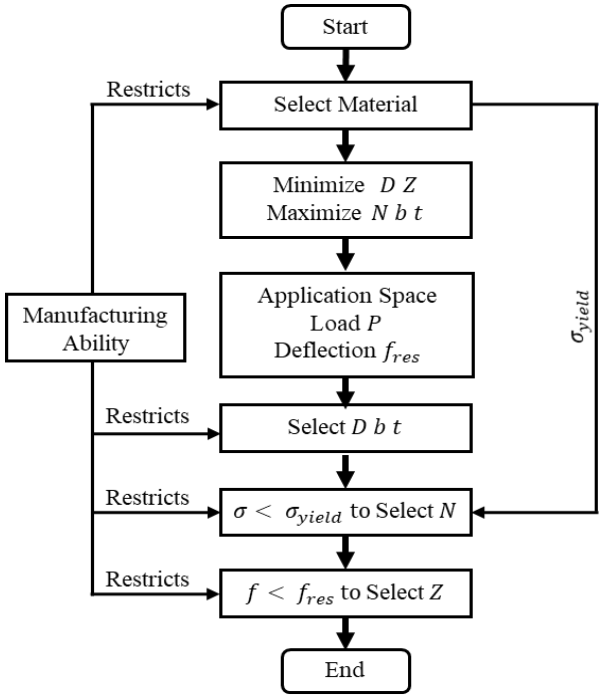

Figure 6: Design flow chart of the wave spring.

so that the inductance of the wave spring is nearly 10 times lower than that of a coil spring with the same dimensions. The optimization of the inductance is investigated using FEM simulations. The total electrical resistance R_e of the compressed wave spring can be written as (where ρ is the electrical resistivity) [13]:

$$R_e = \rho \cdot \frac{l}{A} \cdot \frac{Z}{2N} \cdot C = \rho \cdot \frac{\pi DZ}{4N^2 bt} \cdot C \quad (1)$$

Note that for the thermal resistance as similar equation holds, but now with ρ representing the thermal resistivity. However, as discussed in the next section, the thermal behavior of the proposed spring connector is optimized by using the nut and bolt rather than the spring itself. The manufacturer Smalley provides empirical equations to estimate the stress σ and deflection f [12]:

$$\sigma = \frac{3PD}{2bt^2 N} \tan\left(\frac{\pi}{2N}\right) \quad (2)$$

$$f = \frac{ZK_S PD^3(D-b)}{Ebt^3 N^4 (D+b)} \quad (3)$$

where P is the thrust load and E is Young's Modules of the spring material. The empirical coefficient K_S is determined by the number of waves N ($K_S = 3.88$ for $2.0 \le N \le 4.0$; $K_S = 2.90$ for $4.5 \le N \le 6.5$; $K_S = 2.30$ for $7.0 \le N \le 9.5$; $K_S = 2.13$ for $10.0 \le N$). The spring constant is the

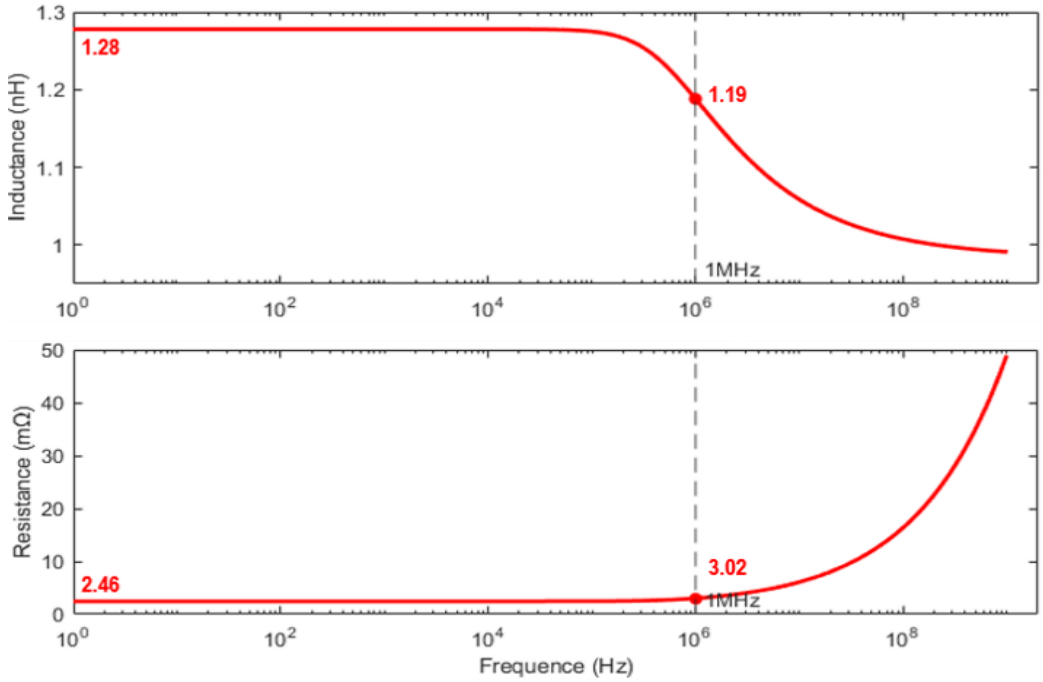

Figure 7: Inductance (top) and resistance (bottom) of the wave spring against frequency.

change of force divided by the change of the deflection. Thus, for the spring constant k the following equation holds:

$$k = \frac{P}{f} = \frac{Ebt^3N^4(D+b)}{ZK_SD^3(D-b)} \quad (4)$$

Fig. 6 shows the design flow chart of the wave spring. The design process consists of the following steps:

1) Beryllium copper ($BeCu_2$) is selected for its high electrical and thermal conductivity.
2) Following (1), minimum D Z and maximum N b t are chosen to minimize the overall electrical resistance of the spring. The influence of parameters on the inductance is analyzed by simulation.
3) The load P and deflection f_{res} are determined by the clearance between the substrates to which the connectors are attached, and the warpage of substrates caused by P.
4) Practical values for D b t of the wave spring are selected, so that the spring can be actually produced by a manufacturer.
5) A maximum N is calculated based on the working stress, which should be less than the material yield stress, (2).
6) Z is identified, considering the overall deformation to be less than the predetermined deformation (3).

Following this design process, an optimized $BeCu_2$ wave spring with flat shims was designed and produced, with optimized parameters enlisted in Table II.

IV. SIMULATION

The parasitics of the optimized wave spring were calculated in ANSYS Q3D [14]. The simulation was performed in a workstation with 12 cores (i7-12700) and 32 Gb random-access memory. Fig. 7 shows the simulation results of the inductance and resistance as a function of the frequency (f), indicating that the spring has a small inductance of 1.28 nH and resistance of 2.46 mΩ from f=1 Hz to 100 kHz. For $f \geq$ 1 MHz, the current starts to flow close to the surface of the metal strips (*i.e.*, skin effect), resulting in an increase in spring resistance and a decrease in inductance. The skin depth δ is the depth at which the current density drops to $1/e$ of its value close to the surface, and can be calculated by:

$$\delta = \sqrt{\frac{1}{\pi f \mu \sigma}} \quad (6)$$

where μ is the magnetic conductivity (1.26×10^{-6} H/m) and σ is the electric conductivity (1.67×10^7 1/Ωm). Thus, the skin depth of the designed beryllium copper connector equals 0.125 mm at f = 1 MHz and is only slightly smaller than the 0.13 mm thickness of wave spring. It demonstrates that the skin effect is not important at 1 MHz in this connector, but makes a great difference to the parasitics for f ~3.6 MHz (see also Fig. 7). The inductance and resistance of the whole connector including the bolt and nut are relatively small, which are 2.94 nH and 3.36 mΩ at 1 MHz, respectively. The wave spring offers a lower resistance and inductance than the typical coil spring due to its physical features, *i.e.* the interconnecting crests. Fig. 8 compares the electrical conductance and inductance of the wave spring connector with those of a conventional counterpart coil spring made out of the same material and having the same dimensions, showing that the wave spring with improved electrical properties is suitable for our envisaged GaN power module.

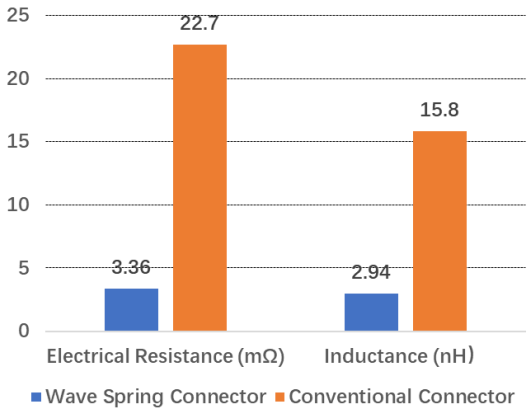

Figure 8: Comparison of electrical properties between those of a conventional coil connector and optimized wave spring connector.

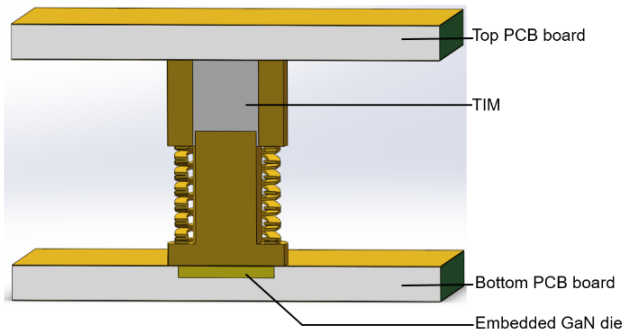

Figure 9: Simulation model for determining the thermal performance of the wave spring.

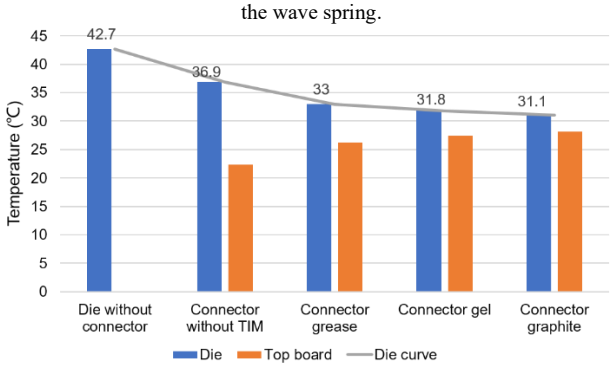

Figure 10: Temperatures of the chip and top bolt for different cooling conditions.

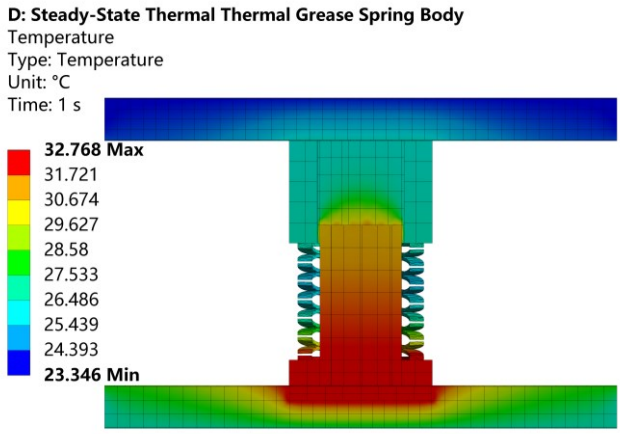

Figure 11: Temperature distribution of the wave spring connector when it cools the embedded die in the bottom PCB.

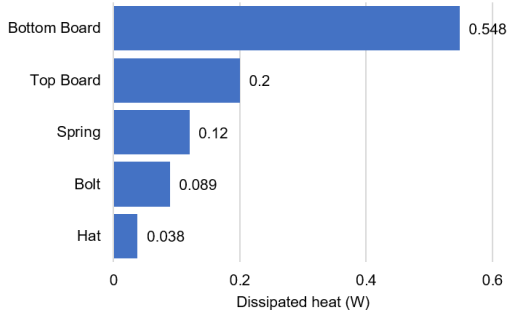

Figure 12: Routes of power dissipation

Although the connector presents an excellent electrical performance, it does not transfer heat efficiently through the spring since the cross section of metal strips is relatively narrow ($\sim 0.07\text{mm}^2$). In order to improve the thermal performance, a thermal interface material (TIM) is used to fill the gap between the bolt and the nut so that heat can be transferred though the middle bar. Fig. 9 presents the

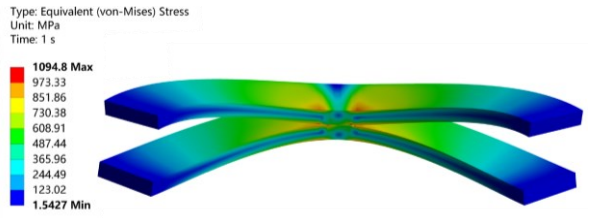

Figure 13: Simulated mechanical stress at a crest of the spring after mechanical loading.

simulation model used for determining the thermal performance, in which a chip with a power loss of 1 W is embedded at the bottom board as a heat source. The environmental temperature is 22 ℃ and the convection coefficient is $0.0001\ \text{W/mm}^2 \cdot ℃$. To analyze the impact of the TIM on the temperature of the chip, five cooling conditions have been investigated: 1) a die without a connector, 2) a connector without TIM, 3) a connector filled with grease ($0.73\ \text{W/m} \cdot \text{K}$), 4) a connector filled with gel ($3\ \text{W/m} \cdot \text{K}$), and 5) a connector filled with graphite ($129\ \text{W/m} \cdot \text{K}$). The temperatures of the chip and top board under these conditions are shown in Fig. 10. Comparing the results of the die without a connector with the one filled with grease, the temperature of the chip at steady state reduces by 10 ℃, revealing that the connector is able to cool the chip effectively. The temperature of the chip using TIM is nearly 4 ℃ lower than that without TIM, indicating that TIM can further improve the cooling ability. Further, the graph shows only a slight fall in the chip temperature using TIM of high thermal conductivity (gel and graphite). It shows that increasing the thermal conductivity of TIM does not significantly improve the thermal performance of connector. Therefore, a silicone compound named Ther-o-Link with thermal conductivity of $0.73\ \text{W/m} \cdot \text{K}$ is selected as TIM in the connectors.

Fig. 11 shows a cross section of the simulated temperature distribution of the optimized spring wave connector with a silicone compound as TIM. Heat flows through the bolt bar to the nut, and only a relatively small part dissipates via the spring. Fig. 12 compares the dissipated power through all components. As can be seen, near 55% of heat dissipates through the bottom PCB, and 20% is transferred through the connector to top PCB, the rest heat dissipates to air via the connector. The simulations indicate that the wave spring connector has an excellent ability of heat conduction and cooling due to the increased surface area and direct-heat-conduction path.

Another important topic is the mechanical behavior of the spring. Generally, the wave spring that is compressed and deforms after the assembly forms the weak part in the module. The critical stress gathers at the crests since the thin metal strips of the spring are subjected to a compressed force of 5 N. Since the wave spring is symmetric, two parts of one third turn are used for the simulation model to emulate the stress after loading (Fig. 13). The maximum stress at the inner edge is 1094.8 MPa, smaller than the yield strength of $BeCu_2$ (Table I). Therefore, it is expected that the optimized wave spring connector will be reliable in operation since the deformation is in the elastic regime. Moreover, the spring is subject to a stress of 487.4 MPa (green area in Fig. 13), which agrees with the working stress of 484.9 MPa calculated from (2), further validating the equations and the parameter optimization process.

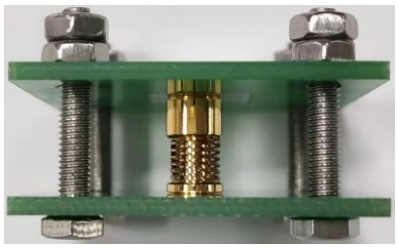

Figure 14: Test PCB boards for determining the electrical resistance of the connector.

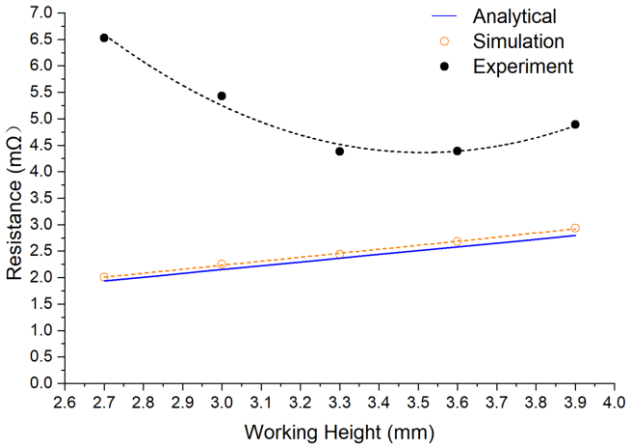

Figure 15: Electrical resistance of wave spring against working height.

V. EXPERIMENT

The resistance of the optimized wave spring is experimentally assessed with PCBs as test boards, as shown in Fig. 14. A layer of gold, the same coating material as on the spring, has been electroplated on the surface of the PCB boards so that the joints form good contacts. The resistance was measured in four-wire mode to eliminate the contribution to the resistance of the measuring leads. The resistances of the connector obtained from (1), FEM and experiment are 3.27 mΩ, 3.36 mΩ, and 5.12 mΩ, respectively. The analytical and FEM results agree quite well, whereas the experiment shows higher values. The difference of 1.76 mΩ between the experimental and simulation results is acceptable, since the total resistance of the connector is in the mΩ range. Part of this difference is likely caused by the inflection of the terminal shims and the surface roughness at the crests. Both will contribute to additional contact resistances, not taken into account in (1) and FEM.

To analyze the impact of contact resistance, a more accurate description for the total resistance of a wave spring is:

$$R = R_{\mathrm{e}} + R_{\mathrm{cc}} + 2 \cdot R_{\mathrm{ct}} = \rho \frac{\pi D}{2N} \cdot \frac{1}{bt} \cdot \frac{Z}{2N} \cdot C + \frac{Z-2}{2N} \cdot R_{\mathrm{cr}} + 2 \cdot R_{\mathrm{ct}} \quad (7)$$

where R_{cr} is the contact resistance at a crest and R_{ct} represents the contact resistance at both spring terminals. In our optimized design the contact resistance is estimated to be ~35% of the total resistance. Fig. 15 shows the resistance of the optimized wave spring without nut and bolt against working height. The resistance is proportional to working height in safe deflection mode. The difference between experimental and analytical resistance is caused by the inflection of terminal shims and the surface roughness at the crests. Therefore, considering the large contact area in the pressure-based joints, further smoothening the contact surface and a reduction of the amount of contact surfaces can reduce this contact resistance. The spring in Fig. 15 was pressed from large to small height. When the working height is less than the designed height (3.3 mm), the high stress at the crests destroys the gold coating layers resulting a high resistance which explains the relatively high resistances in the experiments. Even the spring returns to 3.9 mm, the resistance has increased to 6.7 mΩ because of the destroyed gold coating.

VI. CONCLUSIONS AND FUTURE WORK

This paper proposes an electrical-thermal-mechanical optimized wave spring connector to replace conventional wire bonds in power modules. The connector not only conducts current, but also spreads heat and transfers mechanical load between substrates. The geometrical impact of the wave spring on the electrical resistance has been discussed via analytical expressions and has been validated with FEM simulations. FEM simulations and initial measurement data of the optimized spring connector show a low inductance (~3 nH) and a low resistance (~5 mΩ). In the future, the shape of bolt will be designed such that current and heat can directly flow through the nut to further improve the electrical and thermal performance.

REFERENCES

[1] N. Y. A. Shammas, “Present problems of power module packaging technology”, Microelectron. Reliability, vol. 43, no. 4, pp. 519–527, Apr. 2003.

[2] K. Suganuma, “Interconnection technologies”, in Wide Bandgap Power Semiconductor Packaging, Elsevier, pp. 57–80, 2018.

[3] A. Dutta and S. S. Ang, ‘A module-level spring-interconnected stack power module’, IEEE Trans. Compon. Packag. Manuf. Technol., vol. 9, no. 1, pp. 88–95, Jan. 2019.

[4] J. A. O. Gonzalez, O. Alatise, L. Ran, P. Mawby, P. Rajaguru and C. Bailey, “An initial consideration of silicon carbide devices in pressure-packages”, in Proc. IEEE Energy Conversion Congress and Exposition (ECCE), pp. 1-7, 2016.

[5] N. Zhu, H. A. Mantooth, D. Xu, M. Chen, and M. D. Glover, ‘A Solution to Press-Pack Packaging of SiC MOSFETS’, IEEE Trans. Ind. Electron., vol. 64, no. 10, pp. 8224–8234, Oct. 2017.

[6] C. DiMarino et al., ‘Design and Experimental Validation of a Wire-Bond-Less 10-kV SiC MOSFET Power Module’, IEEE J. Emerg. Sel. Top. Power Electron., vol. 8, no. 1, pp. 381–394, Mar. 2020, doi: 10.1109/JESTPE.2019.2944138.

[7] R. Simpson, A. Plumpton, M. Varley, C. Tonner, P. Taylor and X. Dai, "Press-pack IGBTs for HVDC and FACTs," in CSEE Journal of Power and Energy Systems, vol. 3, no. 3, pp. 302-310, Sept. 2017, doi: 10.17775/CSEEJPES.2016.01740.

[8] Y. Yang, L. Dorn-Gomba, R. Rodriguez, C. Mak, and A. Emadi, ‘Automotive Power Module Packaging: Current Status and Future Trends’, IEEE Access, vol. 8, pp. 160126–160144, 2020, doi: 10.1109/ACCESS.2020.3019775.

[9] S. Eicher *et al*., “4.5 kV press pack IGBT designed for ruggedness and reliability”, in Conference Record of the 2004 IEEE Industry Applications Conference, Seattle, WA, USA, 3, pp. 1534–1539, 2004

[10] C. Chen, F. Luo, and Y. Kang, “A review of SiC power module packaging: Layout, material system and integration”, CPSS Trans. Power Electron. Appl., vol. 2, no. 3, pp. 170–186, Sep. 2017

[11] Y. Pascal, A. Abdedaim, D. Labrousse, M. Petit, S. Lefebvre, and F. Costa, ‘Using Laminated Metal Foam as the Top-Side Contact of a PCB-Embedded Power Die’, IEEE Electron Device Lett., vol. 38, no. 10, pp. 1453–1456, Oct. 2017, doi: 10.1109/LED.2017.2748223.

[12] Smalley, “Ring and spring catalogue and design guide”, USA, 2021, online: https://smalley.dcatalog.com/v/2021-Smalley-Product-Catalog-Metric/.

[13] A. Spaggiari and E. Dragoni, “Multiphysics Modeling and Design of Shape Memory Alloy Wave Springs as Linear Actuators”, J. Mech. Des., vol. 133, no. 6, p. 061008, Jun. 2011.

[14] Ansys Electronics Desktop 2021 R2, Ansys Mechanical 2021 R